J. Mol. Model. **2000**, *6*, 587 – 594

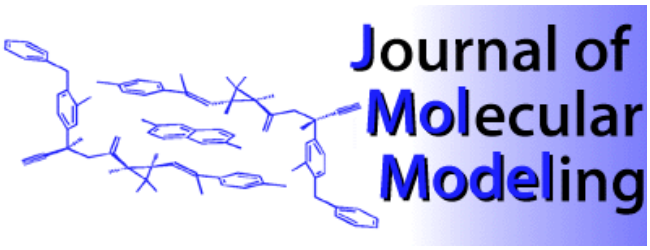

FULL PAPER

Models of the Transmembrane Domains of the Yeast Mitochondrial Citrate Transport Protein

D. Eric Walters and Ronald S. Kaplan

Department of Biochemistry and Molecular Biology, Finch University of Health Sciences/ The Chicago Medical School, 3333 Green Bay Road, North Chicago, IL 60064. Tel.: 847-578-8613; Fax: 847-578-3240.
E-mail: Eric.Walters@FinchCMS.edu

Received: 5 May 2000/ Accepted: 20 June 2000/ Published: 30 November 2000

Abstract We have used cysteine scanning, hydropathy analysis and molecular modeling to construct four possible models of the transmembrane helical domains of the yeast mitochondrial citrate transport protein. Models 1 and 2 invoke the formation of a translocation pathway by the six membrane-spanning alpha-helical domains that comprise each citrate transport protein monomer. Thus the homodimeric CTP (the functional form of the CTP) would contain two separate translocation pathways. Models 3 and 4 explore a novel way in which dimerization might take place, in which transmembrane domain 3 would form part of the dimer interface. This would lead to the formation of two seven-helix translocation pathways within the transporter dimer. Importantly, these studies have led to the construction of the first detailed structural models for any of the mitochondrial anion transport proteins, a family of proteins which is essential to cellular bioenergetics. Furthermore, these models suggest numerous experiments which can be carried out to further elucidate the structure of the translocation pathway through the membrane.

Keywords Hydropathy analysis, α-helix, Helix-helix interaction, Translocation pathway, Membrane protein

Abbreviations CTP, citrate transport protein; MTS, methanethiosulfonate; TMD, transmembrane domain

Running Title Models of Citrate Transport Protein

Introduction

The mitochondrial citrate transport protein (CTP) from higher eukaryotic cells catalyzes an obligatory exchange across the inner mitochondrial membrane of a tricarboxylate (citrate, isocitrate, cis-aconitate) plus a proton, for another tricarboxylate-H^+, or for a dicarboxylate (i.e., malate, succinate), or for phosphoenolpyruvate. [1] Following the movement of citrate out of the mitochondrial matrix through the CTP, the resulting cytoplasmic citrate functions as a carbon source for both the sterol and the fatty acid biosynthetic pathways. [2-5] Furthermore, it provides a source of NAD^+

Correspondence to: D. E. Walters

(*via* the concerted actions of ATP-citrate lyase and malate dehydrogenase) for the glycolytic pathway. It is a member of the mitochondrial inner membrane carrier superfamily.

Because of the primary role of the CTP in higher eukaryotic metabolism, the carrier has been extensively studied. Accordingly it has been purified and reconstituted in liposomal systems, [6,7] kinetically characterized, [8] cloned, [9] and overexpressed. [10] Recently we have extended our investigations to the yeast homologue of the higher eukaryotic protein. [11] An advantage offered by the yeast mitochondrial CTP is that, following overexpression and subsequent purification, transporter function can be reconstituted with high specific activity. Thus, the yeast CTP represents an ideal material for further study. Accordingly, we have embarked upon an extensive program of site-directed mutagenesis in combination with probing mutant function using biochemical and biophysical approaches in order to elucidate the structure-based mechanism for this metabolically important transport protein.

We recently demonstrated [12] that upon isolation, the CTP exists as a functional dimer. Based on hydropathy analysis, [11] each monomer is thought to contain 6 membrane-spanning domains. CTP transmembrane domain 4 (TMD4) is of particular interest for several reasons. First, this domain contains two arginine residues, two glutamines, and an asparagine, so it is not readily identified by hydropathy analysis as a transmembrane domain. Using cysteine scanning mutagenesis in combination with chemical modification of single Cys constructs with hydrophilic MTS reagents, we have demonstrated that TMD4 is α-helical from residues 177-193, [13] and may be α-helical from residue 174. [14] Furthermore, we have defined the aqueous-accessible and -inaccessible faces of this helix using EPR experiments. [14] We have demonstrated [15] *via* site-specific mutagenesis that CTP function requires the presence of positive charge at both Arg-181 and Arg-189 in TMD4. We inferred from these studies that the water-accessible face likely represents a portion of the citrate translocation pathway through the CTP.

Transport proteins having 12 transmembrane domains have previously been modeled by other workers. Two different models were proposed for the glucose transporter GLUT1, [16] each model having a single translocation pathway made up of 5 helices. The intestinal dipeptide transporter PepT1 was also modeled with a single translocation pathway made up of 5 helices. [17] The PepT1 model was used to make predictions (some successful) about the effects of single site mutations. However, the GLUT1 and PepT1 transporters have no homology with the citrate transport protein. In the present paper, we describe the construction of three-dimensional models of the transmembrane helical domains of the mitochondrial citrate transport protein. These represent the first detailed structural models for this family of carrier proteins. Furthermore, they will aid in the design of further site-directed mutagenesis experiments which will contribute to our understanding of the structure-function relationships of this protein.

Table 1 *Transmembrane helical domains identified by hydropathy analysis and, in the case of TMD4, experimentally (Kaplan et al., 2000). Residues in* ***boldface*** *are internal polar/ionic residues which were oriented, as much as possible, toward the translocation path*

TMD1	H_{14}**S**FLAG**S**LAGAA**E**ACI**T**YPF**E**FAK$_{37}$
TMD2	Q_{64}GIG**S**IYVGCPAFIIG**NT**A**K**AGI**R**FLGFD$_{92}$
TMD3	R_{110}GVIAGLGAGLL**ES**VAAV**T***PFE$_{131}$
TMD4	R_{173}GVLPVSM**RQ**AAN**NQ**AV**R**LGCYN$_{194}$
TMD5	**S**$_{214}$GL**T**FLVGAF**S**GIV**T**VY**ST**MPLD$_{236}$
TMD6	R_{276}LG**R**LVL**S**GGIVF**T**IY**EK**VLVMLA$_{299}$

* This residue can face the translocation path in Type 3 and Type 4 models, but not in Type 1 or Type 2

Methods

We previously identified six probable transmembrane helical segments by hydropathy analysis. [11] These segments are listed in Table 1. We have carried out extensive mutation and chemical modification of the residues in TMD4 [13] and have shown that substantially all of this domain is α-helical. These experiments also gave strong indication that the helix is oriented with the N-terminal toward the mitochondrial matrix and the C-terminal toward the cytosol.

In the present work, we have modeled each TMD as a standard α-helix, using the Quanta program (Molecular Simulations Inc., San Diego, CA). The N-terminal nitrogen atom of each helix was capped as an acetamide, and the C-terminal carboxylate of each helix was capped as an N-methylamide, so that energy minimizations would not be distorted by unrealistic electrostatic charges at the termini. Each helix was then subjected to 100-200 cycles of energy minimization using the CHARMm force field [18] to allow adjust-

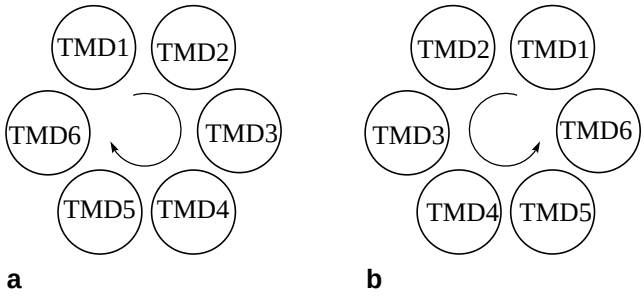

Figure 1 *Schematic representations of Type 1 and Type 2 models. (***a***) In the Type 1 model, the six helices are arranged clockwise when viewed from outside the mitochondrial inner membrane. (***b***) In the Type 2 model, the six helices are arranged counterclockwise when viewed from outside the mitochondrial inner membrane*

Table 2 *Pairs of residues predicted from the Type 1 model to participate in helix-helix interfaces*

TMD1-TMD2	A18-I86, A18-R87, A18-G90, G19-K83, G19-I86, G19-R87, L21-I86, A22-G79, A22-A82, A22-K83, A22-I86, A25-G79, A25-A82, A25-I86, I29-A75, I29-I78, I29-G79, I29-A82, F33-V71, F33-G72, F33-P74, F33-A75
TMD2-TMD3	F88-V112, F88-I113, G85-I113, G85-L116, G85-L120, A84-I113, A84-L116, A84-L120, T81-L116, T81-L120, I77-L120, I77-V124, F76-S123, F76-V124, F76-V127, C73-V124, C73-V127, Y70-T128, I69-V127, I69-T128, I69-E131, I66-T128
TMD3-TMD4	G111-C192, A114-C192, G115-C192, G115-V188, A118-V188, G119-V188, G119-N185, E122-A184, A126-P177, A126-M180, A126-R181, P129-P177, F130-V178, F130-P177
TMD4-TMD5	L190-S214, L190-F218, A187-S214, A187-F218, Q186-F218, Q186-G221, Q186-A222, Q186-G225, Q182-A222, Q182-G225, S179-G225, S179-V229, V178-V229, V178-T232, V175-V229, V175-T232, V175-M233
TMD5-TMD6	L216-A299, T217-V296, T217-A299, V220-L295, V220-V296, V220-A299, G221-V296, F223-L295, S224-V296, S224-L295, S224-E292, V227-F288, S231-F288, S231-G285, S231-G284, L235-V281
TMD6-TMD1	M297-F16, V294-F16, K293-S20, K293-F16, I290-S20, I290-A24, T289-G23, I286-G23, I286-A24, I286-A27, L282-A27, L282-T30, L282-Y31, R279-Y31

ment of backbone conformation around proline residues and to allow any bad sidechain contacts to resolve.

It is expected that the helical segments of the CTP should have hydrophobic faces which interact with the lipid bilayer, and polar or charged residues which should face into the transport pathway to facilitate movement of the charged citrate and isocitrate molecules through the pathway. Table 1 highlights the polar and charged residues which constitute the inward-facing hydrophilic surface for each helix. Our working assumption is that helices will pack next to their sequence neighbors (e.g., TMD4 should pack adjacent to TMD3 and TMD5); this appears reasonable since it has been found that 36 of 37 helices in membrane protein crystal structures are in contact with sequence neighbors. [19]

We considered a number of different ways in which the six helices could be arranged to form a transport pathway. Experimental evidence[12] indicates that the citrate transport protein is a functional dimer. The simplest arrangement would be for each monomer to form a translocation pathway, as shown in Figure 1. As viewed from the external surface of

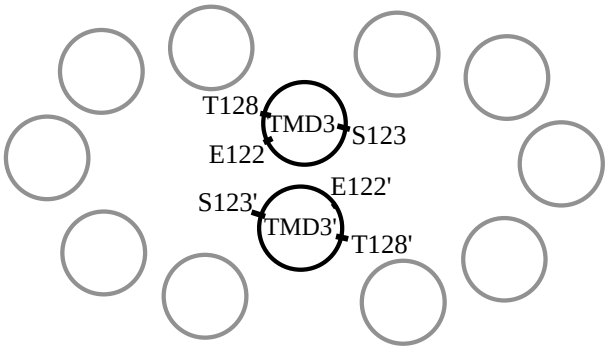

Figure 2 *A way in which TMD3 can form a dimer interface, allowing all three polar residues of each helix to face toward the inside of a translocation pathway*

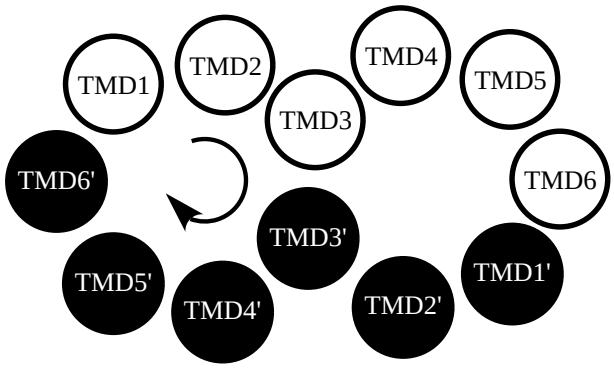

a

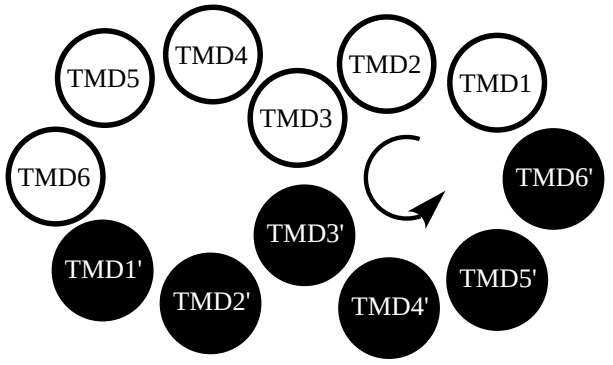

b

Figure 3 *Schematic representations of Type 3 and Type 4 models. TMD3 and TMD3' form an integral part of the dimer interface. (***a***) In the Type 3 model, the helices are arranged clockwise when viewed from outside the mitochondrial inner membrane. (***b***) In the Type 4 model, the helices are arranged counterclockwise when viewed from outside the mitochondrial inner membrane*

the mitochondrion, we modeled this six-helix pathway in both a clockwise arrangement (Type 1 model, Figure 1a) and a counterclockwise arrangement (Type 2 model, Figure 1b). There are numerous ways in which two monomers could associate to form a dimer; we have not yet attempted to model these possibilities.

We noted that TMD3 differs from the other TMDs in that it has only three polar residues (E122, S123, T128) among its internal residues. E122 and S123 are near the center of the helix, while T128 is nearer one end of the helix. It is difficult to place the polar side chains of both E122 and S123 into a single pore because S123 is 100° around the helix from E122, and T128 is predicted to be almost 180° around the helix from S123. For the Type 1 and Type 2 models, we placed E122 and S123 on the hydrophilic surface. But the orientation of these two residues suggested to us the possibility that TMD3 could form part of the dimer interface, as shown in Figure 2. This would lead to the formation of two *seven*-helix pathways, and readily allow placement of the polar side chains of E122 and S123 into adjacent pores. Furthermore, it would allow the T128 side chain to be facing the transport pore. Again, we considered both a clockwise arrangement (Type 3 model, Figure 3a) and a counterclockwise arrangement (Type 4 model, Figure 3b). For the type 3 and type 4 models, two copies of TMD3 were docked as shown in Figure 2. This arrangement places E122 from one helix and serine-123 from the other onto a hydrophilic face which can form part of the transport path. It is interesting that, in the yeast mitochondrial ADP/ATP carrier (another member of the mitochondrial inner membrane carrier superfamily), TMD3 was the only TMD which has no charged residues and showed no second site revertant mutants. [20] This would be

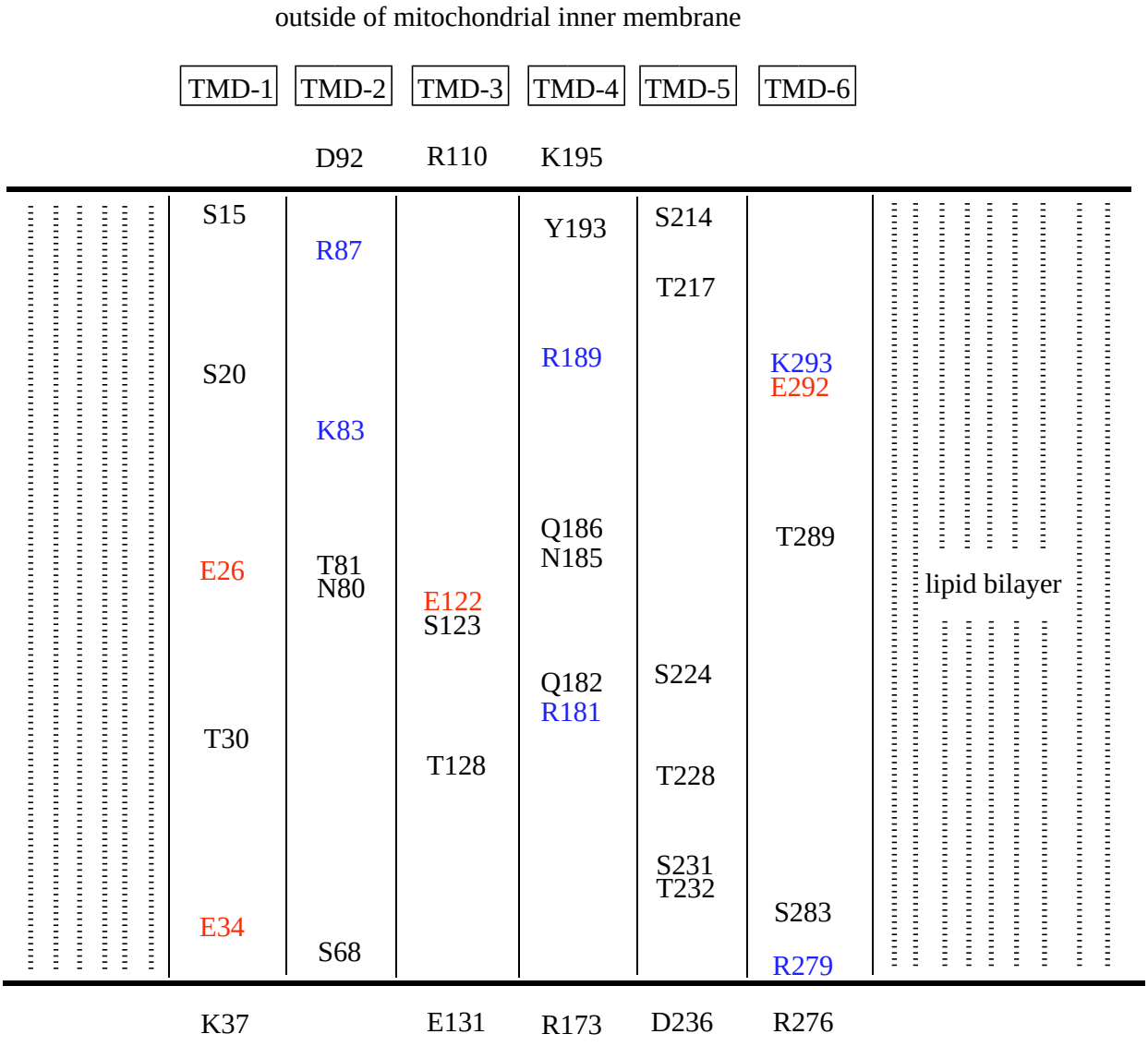

Figure 4 *Schematic view of the placement of polar and charged residues in the translocation path. Positively charged residues in the membrane are in blue, and negatively charged residues in the membrane are in red*

Table 3 *Pairs of residues predicted from the Type 2 model to participate in helix-helix interfaces*

TMD1-TMD2	L17-G85, L17-F88, S20-A84, S20-T81, L21-T81, A24-T81, A27-P74, A27-I77, Y31-P74, Y31-Y70, F35-Y70
TMD2-TMD3	R87-A114, I86-A114, G79-L121, F76-L121, F76-V124, F76-A125, G72-T128, I69-P129
TMD3-TMD4	V112-L190, V112-Y193, G115-R189, G119-Q186, S123-Q186, S123-Q182, A126-Q182, A126-S179, V127-S179, F130-V175
TMD4-TMD5	C192-T217, V188-V220, P177-S231
TMD5-TMD6	S214-M297, G215-M297, F218-M297, F218-V294, F218-K293, F218-I290, A222-V294, A222-I290, G225-I286, I226-I286, V229-I286, V229-S283, V229-L282, T232-L282, T232-R279
TMD6-TMD1	A299-S15, E292-A22, F288-A25, F288-I29, G285-I29, G285-T30, V281-T30, V281-F33, G278-F33, L277-F33

consistent with expectations for a transmembrane helix which must pack with three neighboring helices rather than two.

For all four types of models, helices were manually docked in such a way that the majority of the ionic and polar residues face the interior of the transport pathway, while most of the hydrophobic residues face the lipid bilayer or form helix-helix interfaces. As much as possible, the helices were arranged to maximize favorable steric, electrostatic, and hydrogen bonding interactions. Where necessary, sidechains were rotated to other stable conformers in order to facilitate packing. Following the manual docking, each model (consisting of 6 or 12 helices) underwent 200-400 cycles of energy minimization. At this point, all proline-induced bends were in stable conformations, all serious van der Waals repulsions were relieved, and most electrostatic interactions were energetically favorable.

Results and discussion

Figure 4 shows, schematically, the approximate placement of ionic and polar residues in the translocation path. The translocation path contains 6 positively charged residues. These are, in order from the outside to the inside, R87, R189, K293, K83, R181, and R279. There are 4 negatively charged residues: E292, E26, E122, and E34. All of these have flexible side chains and may exhibit considerable side chain movement during the course of substrate transport. In addition, there are many polar residues: S15, S214, T217, S20, Q186, T289, T81, N185, N80, Q182, S224, S123, T228, T30, T128 (in Type 3 and Type 4 models), S231, T232, S283, and S68. These may interact favorably with the substrate as it passes through the path, and they may help to stabilize different conformations of the charged residues during transport.

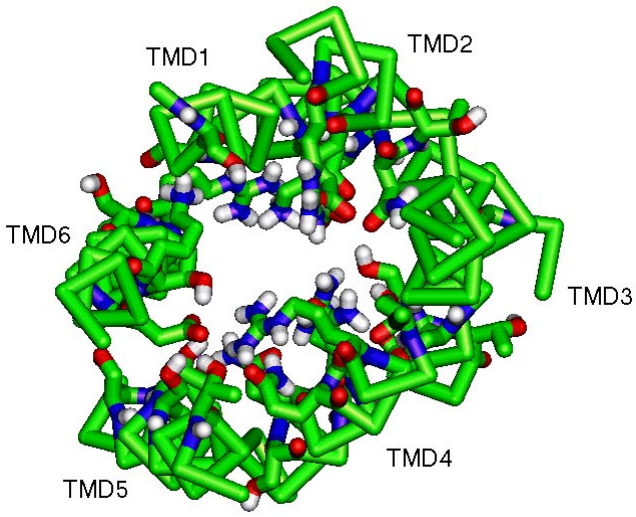

Figure 5 *Type 1 model, viewed from outside the inner mitochondrial membrane. For clarity, only alpha-carbons and intramembrane Arg, Lys, Asp, Glu, Asn, Gln, Ser, and Thr sidechains are shown. Green = carbon, blue = nitrogen, red = oxygen, white = hydrogen*

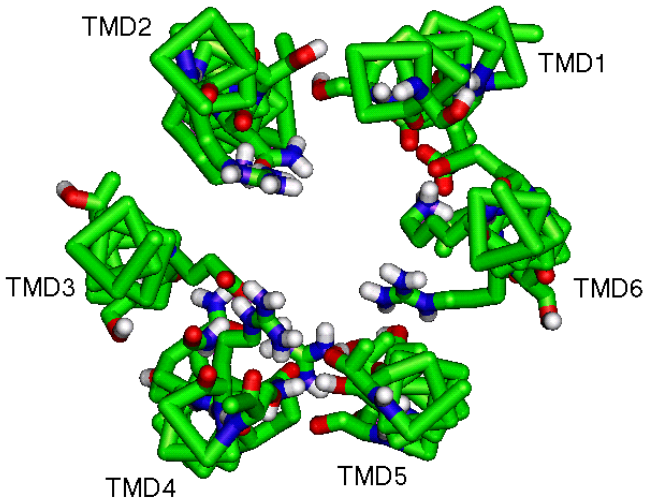

Figure 6 *Type 2 model, viewed from outside the inner mitochondrial membrane. For clarity, only alpha-carbons and intramembrane Arg, Lys, Asp, Glu, Asn, Gln, Ser, and Thr sidechains are shown. Green = carbon, blue = nitrogen, red = oxygen, white = hydrogen*

Table 4 *Pairs of residues predicted from the Type 3 model to participate in helix-helix interfaces*

TMD1-TMD2	
TMD1'-TMD2'	S15-G90, S15-F91, A18-I86, A18-G90, A22-I86, A22-K83, I29-G79, F33-A75, F33-V71
TMD2-TMD3	
TMD2'-TMD3'	F88-V112, F88-I113, G85-I113, A84-I113, A84-L116, T81-I113, T81-L120, I77-L120, I77-L121, I77-V124, C73-V124, C73-V127, Y70-V124, Y70-A125, Y70-T128, I69-V127, I69-T128, I69-E131, I66-T128
TMD3-TMD3'	G111- V112', G111'-V112, G115-G115', G119-G119', G119-E122', G119'-E122, E122-S123', E122'-S123, A126-A126', A126-V127', A126'-V127, V127-F130', V127'-F130, F130-F130'.
TMD3-TMD4	
TMD3'-TMD4'	A114-V188, A114-R189, A114-C192, G117-V188, A118-N185, A118-V188, L121-A184, A125-V178, A125-R181, P129-P177
TMD4-TMD5	
TMD4'-TMD5'	L190-S214, L190-F218, A187-F218, Q186-G221, Q186-S224, Q186-G225, A183-A222, A183-G225, Q182-G225, Q182-V229, S179-V229, V178-T228, V178-T232, V175-V229, V175-T232, V175-M233
TMD5-TMD6	
TMD5'-TMD6'	L216-A299, V220-V296, V220-A299, F223-E292, F223-L295, F223-V296, V227-E292, V227-T289, V227-F288, S231-G285, S231-F288, P234-V281
TMD6-TMD1'	
TMD6'-TMD1	K293-F16, I290-F16, I290-L17, I290-S20, I286-A24, R279-Y31

An important result of the model building is the determination of which amino acid residues make up the interfaces between adjacent helices. The residues which are through-space neighbors constitute predictions that can be tested experimentally by site-directed chemical cross-linking and site-directed spin-labeling. For example, as described below, in the Type 1 model, F33 of TMD1 is predicted to be near V71 and A75 of TMD2, whereas, in the Type 2 model, F33 is predicted to be near V281 of TMD6. A very small number of experiments should be able to distinguish between clockwise

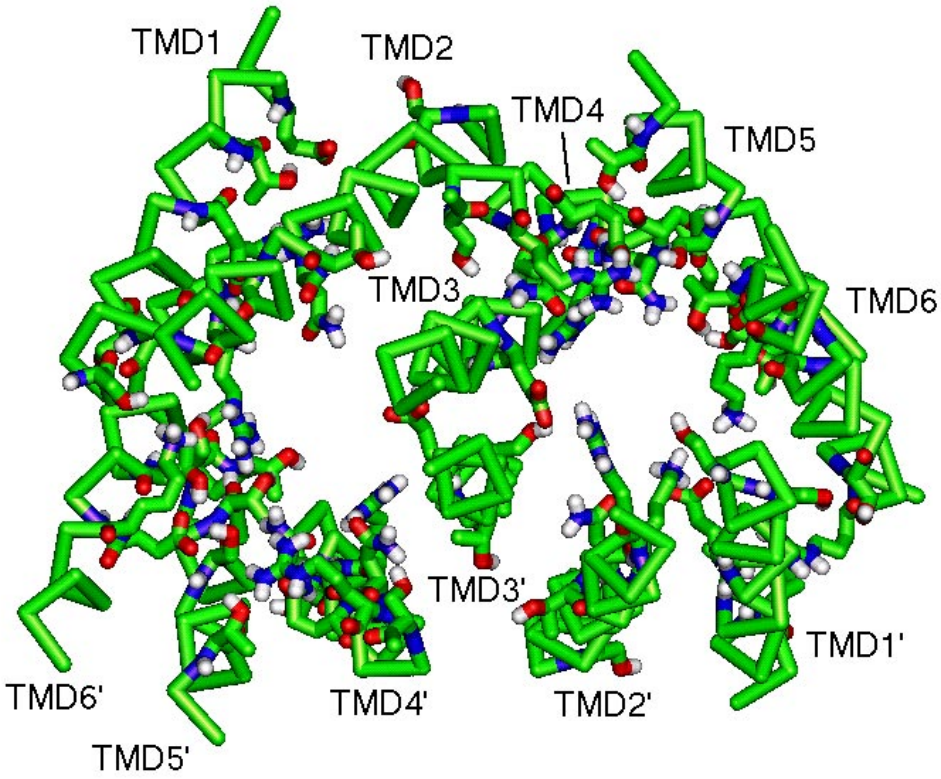

Figure 7 *Type 3 model, viewed from outside the inner mitochondrial membrane. For clarity, only alpha-carbons and intramembrane Arg, Lys, Asp, Glu, Asn, Gln, Ser, and Thr sidechains are shown. Green = carbon, blue = nitrogen, red = oxygen, white = hydrogen*

Table 5 *Pairs of residues predicted from the Type 4 model to participate in helix-helix interfaces*

TMD1-TMD2	
TMD1'-TMD2'	L17-F88, A24-T81, C28-I77, Y31-C73, F35-Y70, F35-I69
TMD2-TMD3	
TMD2'-TMD3'	I86-A114, A82-L121, G79-L121, I78-L121, F76-L121, F76-E122, F76-A125, F76-P129, A75-V124, A75-A125, A75-T128, A75-P129, G72-T128, G72-P129
TMD3-TMD3'	G111- V112', G111'-V112, G115-G115', G119-G119', G119-E122', G119'-E122, E122-S123', E122'-S123, A126-A126', F130-F130'.
TMD3-TMD4	
TMD3'-TMD4'	I113-L190, L116-Q186, L116-R189, L120-R189, L120-Q186, L120-Q182, V127-S179
TMD4-TMD5	
TMD4'-TMD5'	C192-T217, C192-V220, V188-V220, N185-S224, N185-V220, R181-V227, R181-T228, V178-S231, P177-S231, G174-L235
TMD5-TMD6	
TMD5'-TMD6'	S214-M297, G215-M297, F218-M297, F218-V296, F218-V294, F218-K293, A222-I290, G225-I286, I226-I286, V229-I286, V229-S283, V229-L282, T232-L282, M233-R279
TMD6-TMD1'	
TMD6'-TMD1	A299-S15, A299-F16, V296-F16, V296-G19, L295-G19, E292-G23, F288-E26, G285-T30, V281-F33, L277-F33

(Types 1 and 3) and counterclockwise (Types 2 and 4) arrangements. Similarly, experiments on TMD3 should readily indicate whether this helix is part of the dimer interface as proposed by the Type 3 and 4 models.

Type 1 model

In the Type 1 model, the translocation path is formed by six transmembrane helical domains, arranged in a clockwise manner when viewed from the outside of the mitochondrial inner membrane (Figure 1a). Figure 5 illustrates the ionic and polar residues in the translocation path. An α-carbon trace is shown, with side chains shown for arginine, lysine, glutamate, asparagine, glutamine, serine, and threonine. Table 2 lists pairs of residues predicted to be part of helix-helix interfaces in the Type 1 model.

Type 2 model

As in the Type 1 model, the translocation path is formed by six transmembrane helical domains. In the Type 2 model, the helices are arranged counterclockwise as viewed from the outside of the mitochondrial inner membrane (Figure 1b). Figure 6 illustrates the ionic and polar residues in the translocation path. Table 3 lists pairs of residues predicted to be part of helix-helix interfaces in the Type 2 model.

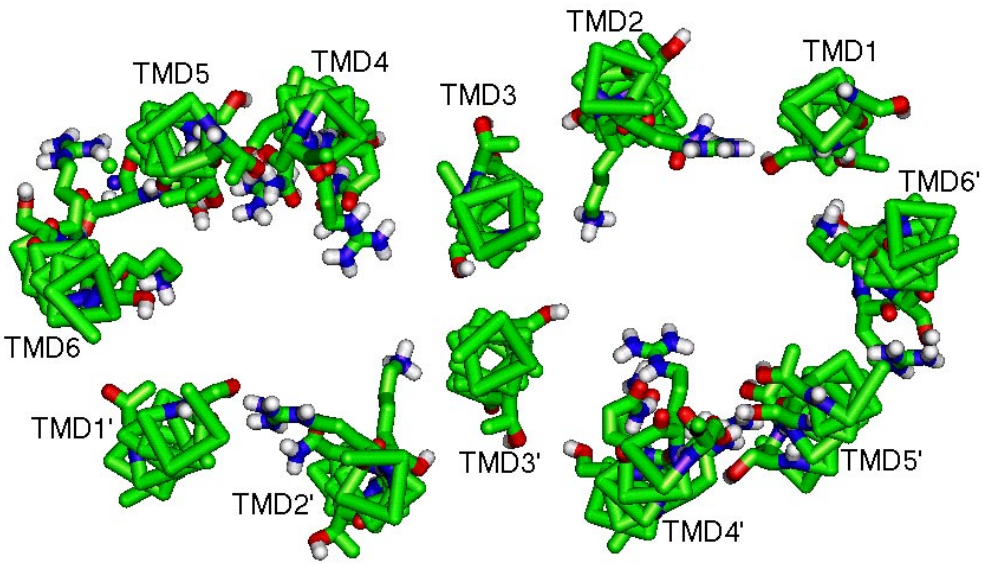

Figure 8 *Type 4 model, viewed from outside the inner mitochondrial membrane. For clarity, only alpha-carbons and intramembrane Arg, Lys, Asp, Glu, Asn, Gln, Ser, and Thr sidechains are shown. Green = carbon, blue = nitrogen, red = oxygen, white = hydrogen*

Type 3 model

For the Type 3 model, TMD3 forms an important part of the dimer interface, packing with TMD2, TMD4, and TMD3' (Figure 3). As in the Type 1 model, helices are arranged clockwise (Figure 3a). We were able to construct a TMD3-TMD3' interface in which there are many favorable hydrophobic packing interactions: G111- V112', G111'-V112, G115-G115', G119-G119', A126-A126', A126-V127', A126'-V127, V127-F130', V127'-F130, and F130-F130'. Table 4 lists pairs of residues predicted to be part of helix-helix interfaces in the Type 3 model. The Type 3 model is shown in Figure 7.

Type 4 model

The Type 4 model, like the Type 3, is dimerized through an interface between TMD3 and TMD3'. Helices are arranged counterclockwise, as shown in Figure 3b. Table 5 lists pairs of residues predicted to be part of helix-helix interfaces in the Type 4 model. The Type 4 model is illustrated in Figure 8.

It is interesting to note that, in packing the helices in the clockwise arrangements (Type 1 and Type 3), the best packing occurred when the helices were tilted about 30°-40° with respect to the axis of the pathway. The counterclockwise arrangements (Type 2 and Type 4) packed better when the helices were essentially parallel to the axes of the pathways.

Conclusion

These studies have led to the construction of the first detailed structural models for any of the mitochondrial anion transport proteins, a family of proteins which is essential to cellular bioenergetics. The models described are being used to design experiments which will aid in the further characterization of the citrate transport protein. The interhelical spatial relationships (i.e. distance and tilt angles) predicted by these models will be tested by engineering single cysteine residues into two separate domains and measuring their separation distance *via* a combination of site-directed chemical cross-linking and site-directed spin-labeling. Moreover, by engineering pairs of cysteine residues, at various positions down the lengths of adjacent helices, we will be able to determine not only the distances between two helices, but their relative tilt angle as well. The experimental distance constraints that are obtained, when used in conjunction with our molecular modeling techniques, will enable the further refinement of a detailed 3-dimensional structural model for the CTP.

Acknowledgment This work was supported by NIH Grant GM-54642 to R.S.K.

Supplementary Material Available. Coordinates for the four models are available, in PDB format, as supplementary material for this paper.

Note: Models can be viewed interactively at http://www.finchcms.edu/biochem/kaplan/ctp_model.html.

References

1. Palmieri, F.; Stipani, I.; Quagliariello, E.; Klingenberg, M. *Eur. J. Biochem.* **1972**, *26*, 587.
2. Watson, J. A.; Lowenstein, J. M. *J. Biol. Chem.* **1970**, *245*, 5993.
3. Endemann, G.; Goetz, P. G.; Edmond, J.; Brunengraber, H. *J. Biol. Chem.* **1982**, *257*, 3434.
4. Brunengraber, H.; Lowenstein, J. M. *FEBS Lett.* **1973**, *36*, 130.
5. Conover, T. E. *Trends Biochem. Sci.* **1987**, *12*, 88.
6. Kaplan, R. S.; Mayor, J. A.; Johnston, N.; Oliveira, D. L. *J. Biol. Chem.* **1990**, *265*, 13379.
7. Bisaccia, F.; De Palma, A.; Palmieri, F. *Biochim. Biophys. Acta* **1989**, *977*, 171.
8. Bisaccia, F.; De Palma, A.; Prezioso, G.; Palmieri, F. *Biochim. Biophys. Acta* **1990**, *1019*, 250.
9. Kaplan, R. S.; Mayor, J. A.; Wood, D. O. *J. Biol. Chem.* **1993**, *268*, 13682.
10. Xu, Y.; Mayor, J. A.; Gremse, D.; Wood, D. O.; Kaplan, R. S. *Biochem. Biophys. Res. Commun.* **1995**, *207*, 783.
11. Kaplan, R. S.; Mayor, J. A.; Gremse, D. A.; Wood, D. O. *J. Biol. Chem.* **1995**, *270*, 4108.
12. Kotaria, R.; Mayor, J. A.; Walters, D. E.; Kaplan, R. S. *J. Bioenerg. Biomembr.* **1999**, *31*, 543.
13. Kaplan, R. S.; Mayor, J. A.; Brauer, D.; Kotaria, R.; Walters, D. E.; Dean, A. M. *J. Biol. Chem.* **2000**, *275*, 12009-12016.
14. Kaplan, R. S.; Mayor, J. A.; Kotaria, R.; Mchaourab, H. S. *Biochem.* **2000**, *39*, 9157-9163.
15. Xu, Y.; Kakhniashvili, D. A.; Gremse, D. A.; Wood, D. O.; Mayor, J. A.; Walters, D. E.; Kaplan, R. S. *J. Biol. Chem.* **2000**, *275*, 7117-7124.
16. Zeng, H.; Parthasarathy, R.; Rampal, A. L.; Jung, C. Y. *Biophys. J.* **1996**, *70*, 14.
17. Bolger, M. B.; Haworth, I. S.; Yeung, A. K.; Ann, D.; von Grafenstein, H.; Hamm-Alvarez, S.; Okamoto, C. T.; Kim, K.-J.; Basu, S. K.; Wu, S.; Lee, V. H. L. *J. Pharm. Sci.* **1998**, *87*, 1286.
18. Brooks, B. R.; Bruccoleri, R. E.; Olafson, B. D.; States, D. J.; Swaminathan, S.; Karplus, M. *J. Comp. Chem.* **1983**, *4*, 187.
19. Bowie, J. U. *J. Mol. Biol.* **1997**, *272*, 780.
20. Nelson, D. R.; Douglas, M. G. *J. Mol. Biol.* **1993**, *230*, 1171.